ISIJ International, Vol. 52 (2012), No. 10, pp. 1894–1901

Effects of the Addition of Cr, Mo and Ni on the Microstructure and Retained Austenite Characteristics of 0.2% C–Si–Mn–Nb Ultrahigh-strength TRIP-aided Bainitic Ferrite Steels

Junya KOBAYASHI,[1)]* Daiki INA,[1)] Nobuo YOSHIKAWA[1)] and Koh-ichi SUGIMOTO[2)]

1) Graduate Student, Shinshu University, 4-17-1, Wakasato, Nagano, 380-8553 Japan. E-mail: ina@sugimotolab.shinshu-u.ac.jp, yoshikawa@sugimotolab.shinshu-u.ac.jp 2) Department of Mechanical Systems Engineering, Shinshu University, 4-17-1, Wakasato, Nagano, 380-8553 Japan. E-mail: sugimot@shinshu-u.ac.jp

(*Received on March 16, 2012; accepted on May 28, 2012*)

Cr, Mo and/or Ni were added to *TRIP-aided bainitic ferrite* (TBF) steel (0.2% C, 1.5% Si, 1.5% Mn and 0.05% Nb ultrahigh-strength TBF steel) in order to increase its hardenability. In addition, the effects of the alloying elements on the Vickers hardness, microstructure and retained austenite characteristics of the TBF steels were investigated. When the TBF steels were austempered at temperatures between M_S and M_f, the Vickers hardness increased from HV300 to HV430 with increasing hardenability. The microstructure consisted of martensite and bainitic ferrite lath structures and retained austenite phases and the volume fraction of retained austenite increased with increasing hardenability. Conversely, the carbon concentration of the retained austenite decreased with increasing hardenability. Simultaneously, the quantity of the hard blocky martensite phase (M-A constituent) with refined interlath retained austenite films increased with increasing hardenability. These characteristics are mainly caused by the delayed bainite transformation during austempering through the addition of Cr, Mo and/or Ni. The addition of Ni lowered the T_0 line further. The retained austenite phases of Cr- and/or Mo-bearing TBF steels were relatively stable against straining, despite their low carbon concentrations.

KEY WORDS: TRIP-aided steel; ultrahigh-strength steel; microstructure; bainitic ferrite; martensite; retained austenite; hardenability.

1. Introduction

The transformation-induced plasticity (TRIP)[1)] of metastable retained austenite significantly improves the formability of steels. In the past decade, second- and third-generation advanced high-strength steels such as 5–25% Mn twinning-induced plasticity (TWIP)/TRIP steels,[2–4)] quench and partitioning (Q&P) steel[5)] and TRIP-aided steel with a bainitic ferrite lath structure matrix (*TRIP-aided bainitic ferrite steel*; TBF steel) have been developed in order to reduce the automotive body-in-white weight and to improve impact safety. TBF steel possesses not only a good combination of ultrahigh strength and stretch flangeability, but also a high fatigue strength, high impact energy, and good hydrogen embrittlement performance because of the metastable retained austenite.[6–10)] Thus, it is expected that TBF steel can also be applied to some automotive driving parts. In this case, high hardenability is required, because TBF sheet steel, which has been developed recently, hardly contains any alloying elements except for Si and Mn.

Up to now, many papers have reported the effects of Si, Mn, Al and Nb on the retained austenite characteristics of TBF steel.[6–10)] However, the effects of alloying elements such as Cr, Mo and Ni, which enhance hardenability, on the microstructure and retained austenite characteristics of TBF steel have not yet been investigated.

In this study, for the development of a new type of TBF steel with good hardenability, the effects of additions of Cr, Mo and/or Ni on the Vickers hardness, microstructure, and retained austenite characteristics in a 0.2% C, 1.5% Si, 1.5% Mn and 0.05% Nb TBF steel were investigated.

2. Experimental Procedure

In this study, five kinds of 100-kg steel ingots with different Cr, Mo and Ni contents were prepared by vacuum melting followed by hot-forging, to produce bars of 32 mm in diameter. Subsequently, the bars were heated to 1 200°C and hot-rolled to 13 mm in diameter with a finishing rolling temperature of 850°C, and then cooled in air to room temperature before annealing at 650°C. The chemical compositions of the steels are detailed in **Table 1**, with the martensite start temperature (M_S, °C) estimated by the following equation:[11)]

* Corresponding author: E-mail: koba@sugimotolab.shinshu-u.ac.jp
DOI: http://dx.doi.org/10.2355/isijinternational.52.1894

Table 1. Chemical compositions (mass%), estimated martensite start temperatures (M_S, °C) and hardenability factors (Πf_i) of steels A–E.

Steel	C	Si	Mn	P	S	Al	Nb	Cr	Mo	Ni	N	O	M_S	Πf_i
A	0.20	1.54	1.53	0.005	0.0005	0.039	0.049	–	–	–	0.0007	0.0007	419	14.6
B	0.21	1.49	1.50	0.004	0.0019	0.040	0.050	0.50	–	–	0.0012	0.0012	407	30.6
C	0.20	1.49	1.50	0.004	0.0019	0.040	0.050	1.00	–	–	0.0012	0.0012	397	47.0
D	0.18	1.48	1.49	0.004	0.0029	0.043	0.050	1.02	0.20	–	0.0010	0.0015	407	76.8
E	0.21	1.49	1.49	0.003	0.0019	0.034	0.049	1.00	0.20	1.52	0.0014	0.0009	370	135.8

$$M_S\ (°C) = 550 - 361 \times (\%C) - 39 \times (\%Mn) - 17 \times (\%V) - 20 \times (\%Cr) - 17 \times (\%Ni) - 10 \times (\%Cu) - 5 \times (\%Mo + \%W) - 0 \times (\%Si) + 15 \times (\%Co) + 30 \times (\%Al) \quad (1)$$

where *%C*, *%Mn*, *%Si*, *%P*, *%S*, *%V*, *%Cr*, *%Ni*, *%Cu*, *%Mo*, *%W*, *%Co* and *%Al* represent the added contents (mass%) of the individual alloying elements.

In this study, the hardenability of these steel bars is defined by the product of the multiplying factors (Πf_i) or the Grossman pearlitic hardenability factor,[12,13] because they contain boron with many alloying elements for hardenability. Πf_i was calculated using the following equation.

$$\Pi f_i = D_I/D_I^* = (1 + 0.64\%Si) \times (1 + 4.1\%Mn) \times (1 + 2.83\%P) \times (1 - 0.62\%S) \times (1 + 2.33\%Cr) \times (1 + 0.52\%Ni) \times (1 + 3.14\%Mo) \times (1 + 0.27\%Cu) \times (1 + 1.5(0.9 - \%C)) \quad (2)$$

where D_I and D_I^* are the ideal critical diameters for the hardenability of alloying and carbon steels, respectively. The effect of the prior austenitic grain size in Eq. (2) is excluded. The last term on the right-hand side in Eq. (2) is applied only for steel containing boron. Hereafter, Πf_i is called the "hardenability factor." The continuous cooling transformation (CCT) diagrams of steels A–E are shown in **Fig. 1**.

Specimens with diameters of 13 mm and lengths of 10 mm were used for the heat treatment illustrated in **Fig. 2**, that is, annealing at 900°C for 1 200 s in the austenite region, and subsequent austempering at T_A = 350, 400 or 450°C for t_A = 100, 1 000 or 10 000 s, respectively. The bainitic transformation behavior of the steels was measured by experimental dilatometry.

The retained austenite characteristics of the TBF steels were investigated by X-ray diffractometry. The specimen surfaces were electropolished after grinding with Emery paper (#1200). The volume fraction of retained austenite (f_γ, vol%) was quantified from the integrated intensity of the (200)α, (211)α, (200)γ, (220)γ and (311)γ peaks obtained by X-ray diffractometry using Mo-Kα radiation.[14] The carbon concentration (C_γ, mass%) was estimated from the equation below. In this case, the lattice constant (a_γ, $\times 10^{-1}$ nm) was measured from the (200)γ, (220)γ and (311)γ peaks with Cu-Kα radiation.[15]

$$a_\gamma = 3.5780 + 0.0330C_\gamma + 0.00095Mn_\gamma - 0.0002Ni_\gamma + 0.0006Cr_\gamma + 0.0220N_\gamma + 0.0056Al_\gamma - 0.0004Co_\gamma + 0.0015Cu_\gamma + 0.0031Mo_\gamma + 0.0051Nb_\gamma + 0.0039Ti_\gamma + 0.0018V_\gamma + 0.0018W_\gamma \quad (3)$$

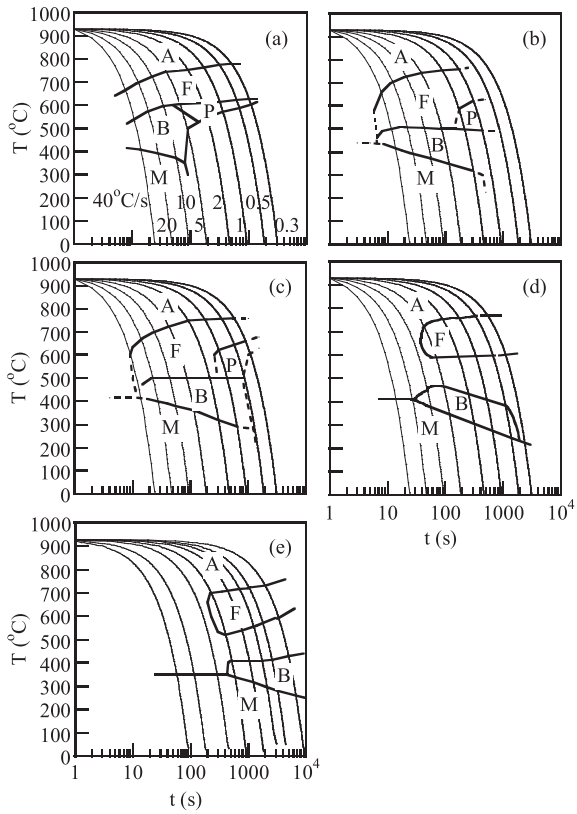

Fig. 1. Measured CCT diagrams of steels (a) A, (b) B, (c) C, (d) D and (e) E, in which A, F, P, B and M represent austenite, ferrite, pearlite, bainite and martensite, respectively.

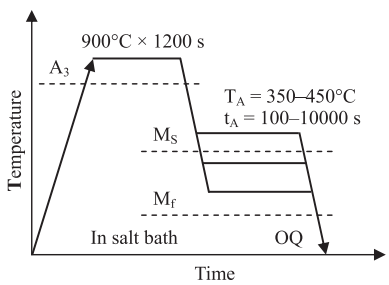

Fig. 2. Heat-treatment diagram of steels. OQ: quenching in oil.

where Mn_γ, Ni_γ, Cr_γ, N_γ, Al_γ, Co_γ, Cu_γ, Mo_γ, Nb_γ, Ti_γ, V_γ and W_γ represent the concentrations of the respective individual elements (mass%) in the retained austenite. As an approximation, the contents of added alloying elements were substituted for these concentrations in this study.

The microstructures were observed by TEM (transmission electron microscopy), field-emission scanning electron

microscopy (FE-SEM) and FE-SEM electron backscatter diffraction pattern (FE-SEM-EBSP) analysis. Specimens for FE-SEM were etched with 5% nital etchant. Specimens for FE-SEM-EBSP were finished with colloidal silica after polishing with γ-alumina particles.

Vickers hardness tests were carried out using a Vickers microhardness machine at 25°C with a load of 0.98 N. The surface of the specimen was polished with Emery paper (#600).

3. Results

3.1. Vickers Hardness

Figure 3 shows the Vickers hardnesses of steels A–E austempered at T_A = 350, 400 or 450°C for 1 000 s as a function of hardenability factor. The TBF steels have a Vickers hardness of about HV330–430 when austempered at 350°C, although this is decreased by austempering at 400°C. The Vickers hardness increases with increasing hardenability factor. When the TBF steels are austempered at 450°C, the Vickers hardnesses increase significantly, particularly in steels C–E.

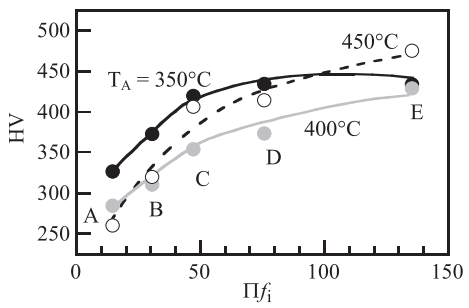

Fig. 3. Vickers hardness as a function of hardenability factor (Πf_i) in steels A–E austempered at 350, 400 or 450°C for 1 000 s.

3.2. Microstructure

The dilatation and volume fraction of the transformed phase in steels A and D austempered at 400°C are shown in **Fig. 4**. The volume fraction is corrected and normalized

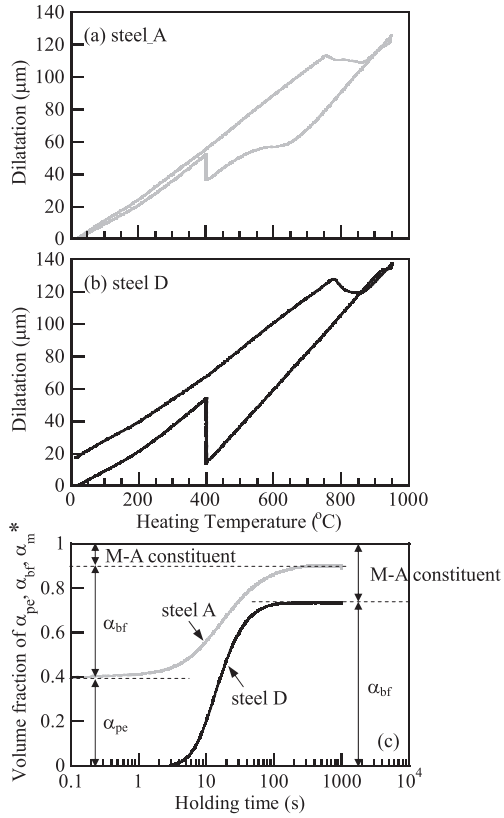

Fig. 4. Dilatation curves during heating of steels (a) A and (b) D, and (c) volume fractions of each phase in steels A and D during austempering after austenitizing, in which α_{pe} and α_{bf} are pro-eutectoid ferrite and bainitic ferrite, respectively.

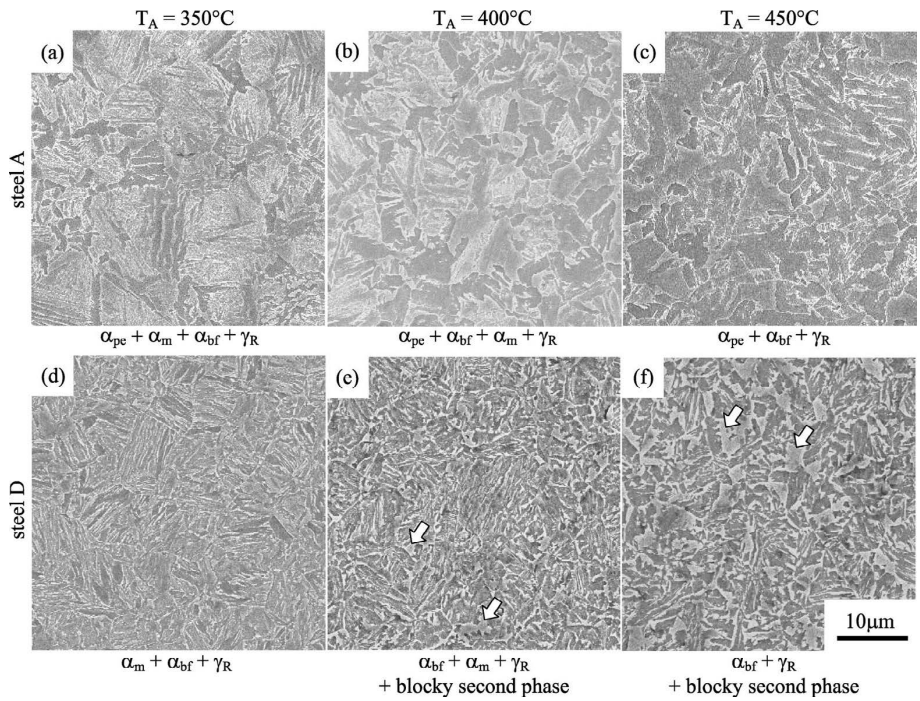

Fig. 5. Typical SEM images of steels A and D subjected to austempering at 350, 400 and 450°C for 1 000 s, in which α_{pe}, α_{bf}, α_m and γ_R are pro-eutectoid ferrite, bainitic ferrite, martensite and retained austenite, respectively. Arrows indicate blocky second phase or M-A constituent.

according to the SEM image of the microstructure. In steel A, the ferritic transformation takes place below 700°C (Fig. 4(a)), which is different from that in steel D (Fig. 4(b)). This indicates that a large amount of pro-eutectoid ferrite is formed during cooling. The formation behavior of the M-A constituents in both steels A and D appears immediately after quenching from 400°C. In Fig. 4(c), the bainite transformation start time of steel A is slightly sooner than that of steel D. However, the bainite transformation in both steels is saturated at 1 000 s.

Typical SEM images of steels A and D austempered at 350, 400 or 450°C are presented in **Fig. 5**. When steel A is austempered at 400 or 450°C, the microstructures consist of bainitic ferrite and pro-eutectoid ferrite. If the steel is austempered at 350°C, the volume fractions of martensite and bainitic ferrite lath structures increase, with a small amount of pro-eutectoid ferrite.

On the other hand, when steel D is austempered at 350°C,

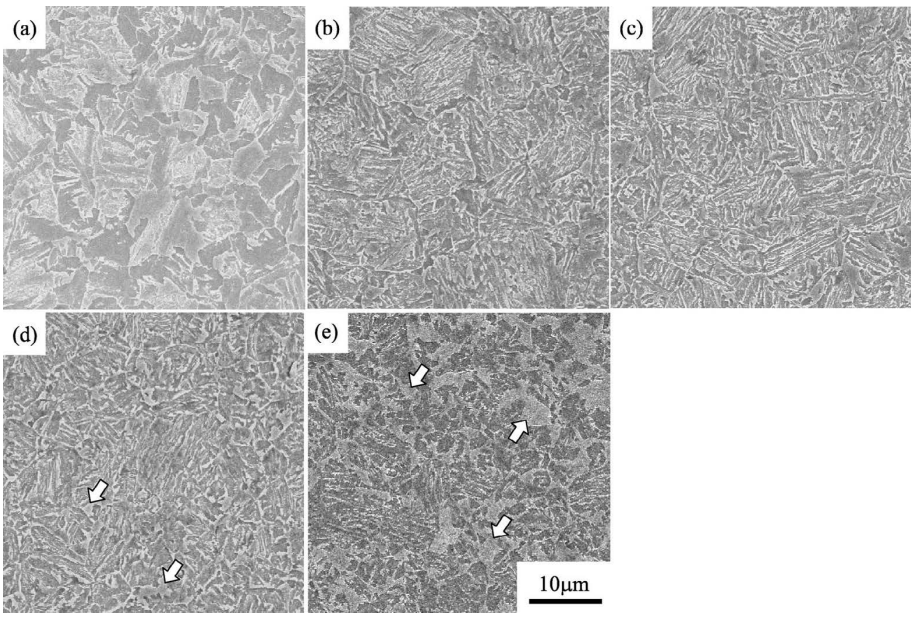

Fig. 6. Typical SEM images of steels (a) A, (b) B, (c) C, (d) D and (e) E austempered at 400°C for 1 000 s. Arrows indicate blocky second phase or M-A constituent.

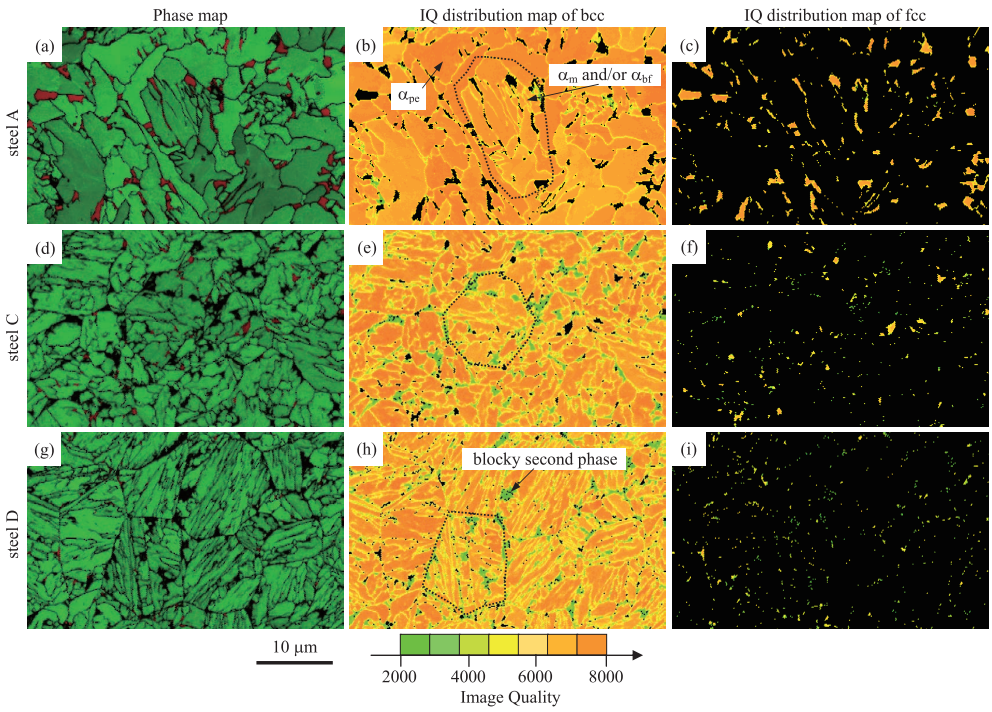

Fig. 7. Phase maps and image-quality (IQ) distribution maps of matrix (bcc) and retained austenite (fcc) in steels A, C and D austempered at 400°C for 1 000 s. In (a), (d) and (g), the green and red phases denote the matrix structure (bcc) and retained austenite (fcc), respectively. In (b), (e) and (h), the yellowish-green phase is the blocky second phase or M-A constituent, in which α_{pe}, α_{bf} and α_m are pro-eutectoid ferrite, bainitic ferrite and martensite, respectively. The prior austenitic grain boundary is illustrated as a dotted line. In (c), (f), and (i), the darker yellow regions represent structures with a higher image-quality index, and the black phases are other structures.

i.e., below the M_S temperature, the matrix structure changes to a mixture of bainitic ferrite and martensite lath structures. From the work of Sugimoto *et al.*,[7,8] as the austempering temperature decreases, the amount of martensite lath structure ($f\alpha_m$) increases according to the following equation:[16]

$$f\alpha_m = 1 - \exp\{-0.011(M_S - T_A)\} \quad (4)$$

It is worth noting that a large amount of a blocky second phase is formed when steel D is austempered at 400 or 450°C.

Figure 6 shows typical SEM images of steels A–E austempered at 400°C, and the results of phase maps and image-quality distribution maps for steels A, C and D austempered at 400°C are given in **Fig. 7**. Comparing the SEM-EBSP analyses of steels A and C, it is found that steel C possesses a uniform and fine lath matrix structure and a larger amount of the blocky second phase (Figs. 7(d) and 7(e)). The blocky second phase (yellowish-green regions in Figs. 7(e) and 7(h)) is located on the prior austenitic grain boundary and prior packet boundary. This looks like a narrow lath martensite structure with fine retained austenite because the image-quality index is relatively low. This indicates that the blocky second phase corresponds to the M-A constituent. The volume fraction of the blocky second phase also increases linearly with increasing hardenability factor, as seen in **Fig. 8**. On the other hand, the volume fraction of the retained austenite is saturated to about 13 vol% in steels C, D and E.

From Fig. 7, it is found that most of the retained austenite in steel A is typically located on the bainitic ferrite lath boundary or prior austenitic grain boundary. With increasing hardenability, the retained austenite is mainly surrounded by or adjacent to the narrow lath martensite in the blocky second phase. As a result, the retained austenite is considerably refined. It is noteworthy that the retained austenite of steels C–E has lower image-quality indexes than that of steel A (Figs. 7(c), 7(f) and 7(i)). The lower image-quality index of the retained austenite is caused by the increased dislocation density, as well as by the refining of the retained austenite. In addition, since the retained austenite is formed in the blocky second phase with a lower image-quality index, the image-quality index of the retained austenite is lowered. This lower image-quality index indicates that the retained austenite in steels C–E may possess a higher dislocation density compared with that in steel A.[17]

In **Fig. 9**(a), it is seen that cementites never precipitate in the bainitic ferrite lath structure matrix of steel B austempered at 350°C, which is similar behavior to that of steel D austempered at 400°C (Fig. 9(b)). In steel D, the retained austenite films are surrounded by or adjacent to the narrow lath martensite in the blocky second phase.

3.3. Retained Austenite Characteristics

Figures 10 and **11** show the initial volume fractions and carbon concentrations of the retained austenite of steels A–E austempered for different austempering times and at different temperatures as a function of the hardenability factor. In Fig. 10, with the exception of steels A and B, the volume fraction of the retained austenite is found to be highest when austempering is performed for 1 000 s. The carbon concentration of the retained austenite hardly changes for austempering times of 1 000 and 10 000 s, although it decreases with increasing hardenability factor. As a result, the total carbon concentration of the retained austenite decreases with increasing hardenability factor.

From Fig. 11, it is found that the volume fraction of the retained austenite also increases with increasing hardenability factor when austempered at 350 or 400°C. In contrast, the carbon concentration of the retained austenite decreases with increasing hardenability factor. When steels A–E are austempered at 450°C, the retained austenite characteristics deteriorate considerably, especially for steels D and E with high hardenability factors.

According to previous studies,[6,7] the retained austenite stability against straining of the TBF steel can be evaluated by the "*strain-induced transformation factor*, *k*", defined by the equation below, rather than by the carbon concentration, if the retained austenite morphology changes significantly:

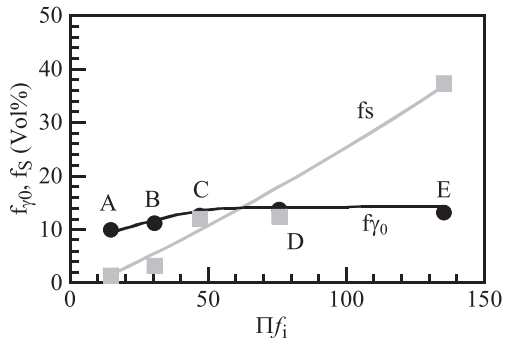

Fig. 8. Variations in volume fractions of retained austenite ($f_{\gamma 0}$) and blocky second phase or M-A constituent (f_s) as a function of hardenability factor (Πf_i) in steels A–E austempered at 400°C for 1 000 s.

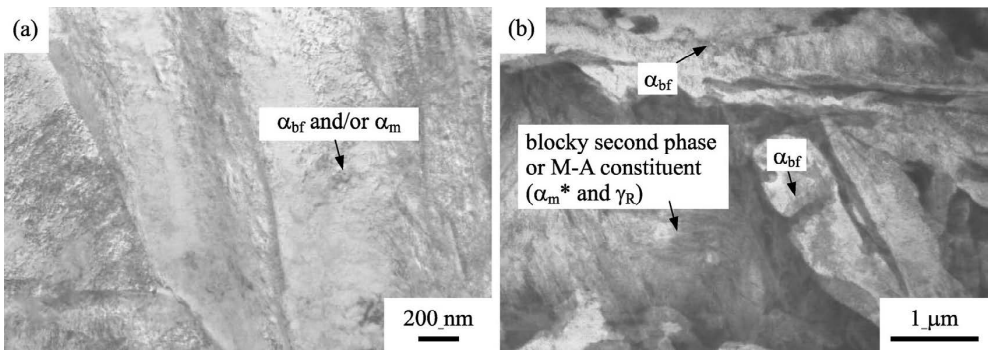

Fig. 9. TEM images of (a) steel B austempered at 350°C and (b) steel D austempered at 400°C for 1 000 s, in which α_{bf}, α_m, α_m* and γ_R are bainitic ferrite, wide lath martensite, narrow lath martensite and retained austenite, respectively.

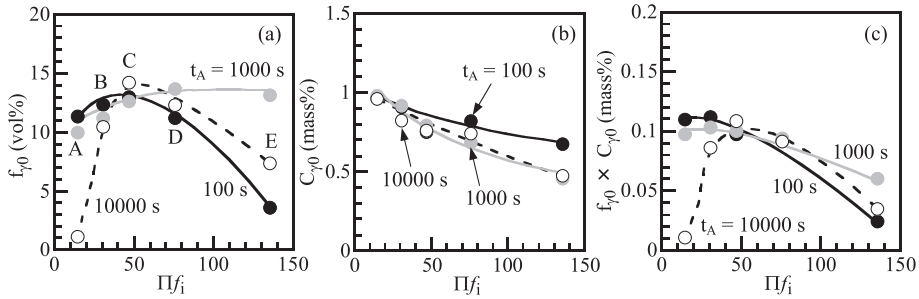

Fig. 10. Variations in (a) initial volume fraction ($f_{\gamma 0}$), (b) initial carbon concentration ($C_{\gamma 0}$) and (c) total carbon concentration ($f_{\gamma 0} \times C_{\gamma 0}$) of retained austenite as a function of hardenability factor (Πf_i) in steels A–E austempered at 400°C for 100, 1 000 or 10 000 s.

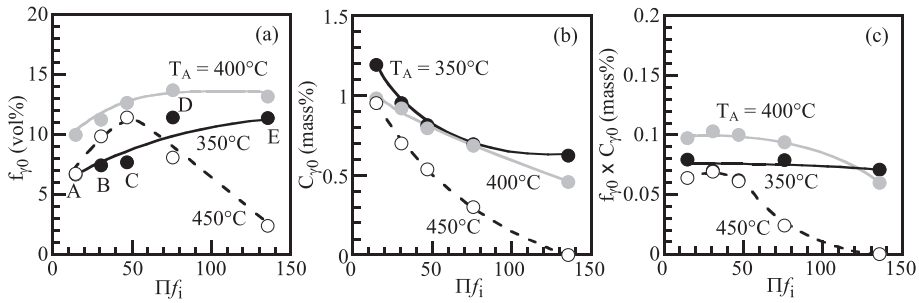

Fig. 11. Variations in (a) initial volume fraction ($f_{\gamma 0}$), (b) initial carbon concentration ($C_{\gamma 0}$) and (c) total carbon concentration ($f_{\gamma 0} \times C_{\gamma 0}$) of retained austenite as a function of hardenability factor (Πf_i) in steels A–E austempered at 350, 400 or 450°C for 1 000 s.

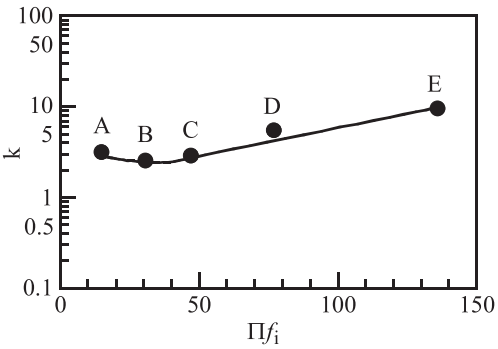

Fig. 12. Variation in k value as a function of hardenability (Πf_i) in steels A–E austempered at 400°C for 1 000 s.

$$\log f_\gamma = \log f_{\gamma 0} - k\varepsilon \quad (5)$$

where f_γ is the volume fraction of the retained austenite after being strained under a plastic strain ε, and $f_{\gamma 0}$ is the initial volume fraction of the retained austenite. A lower k value means a high retained austenite stability. The retained austenite stabilities of steels A–E austempered at 400°C for 1 000 s are shown in **Fig. 12**. Although the carbon concentration of the retained austenite decreases significantly with increasing hardenability factor, the k values of the steels increase slightly with increasing hardenability.

4. Discussion

4.1. Effects of Chemical Composition on Microstructure

In Figs. 4 to 9, the blocky second phase or M-A (martensite-austenite) constituent in steels B–E increased when they were austempered at 350 or 400°C, particularly in the steels with higher hardenability factors. Because the retained austenite possessed a lower image-quality index than the initial wide lath martensite formed upon austempering (Figs. 7(f) and 7(i)), the phase was considered to have a higher dislocation density (or higher flow stress). In addition, most of the retained austenite was located in the blocky second phase and on the prior austenitic grain boundary.

From the above observations, the microstructural changes during austempering in steels A and D austempered at 350 or 400°C (lower than the M_S temperature) are illustrated in **Fig. 13**. In steel A with low hardenability, part of the austenite first transforms to pro-eutectoid ferrite (α_{pe}) during cooling, and then to martensite (α_m) in stage 2 of Fig. 13(a). The volume fraction of martensite increases with decreasing austempering temperature, as calculated by the Koistinen–Marburger equation (Eq. (4)). The supersaturated solute carbon in lath martensite is immediately partitioned to the austenite during successive austempering, until the M_S temperature of the carbon-enriched austenite decreases below the initial M_S temperature. As a result, the bainite transformation starts and is accelerated because of an increase in the interface between the initially transformed martensite and the pro-eutectoid ferrite.[18,19] In addition, in stages 3 and 4, the carbon concentration of the retained austenite increases with the transformation from untransformed austenite to bainitic ferrite. The carbon concentration of the retained austenite is enriched to T_0 or T_0', at which point austenite and ferrite with the same chemical compositions have identical free energies.[20]

In steel D with a higher hardenability factor, the bainite transformation and carbon diffusion are delayed (Figs. 2(d) and 4(c)). In addition, the difference between the M_S and austempering temperatures is small (7°C), so that the volume fraction of the martensite calculated by Eq. (4) is 7

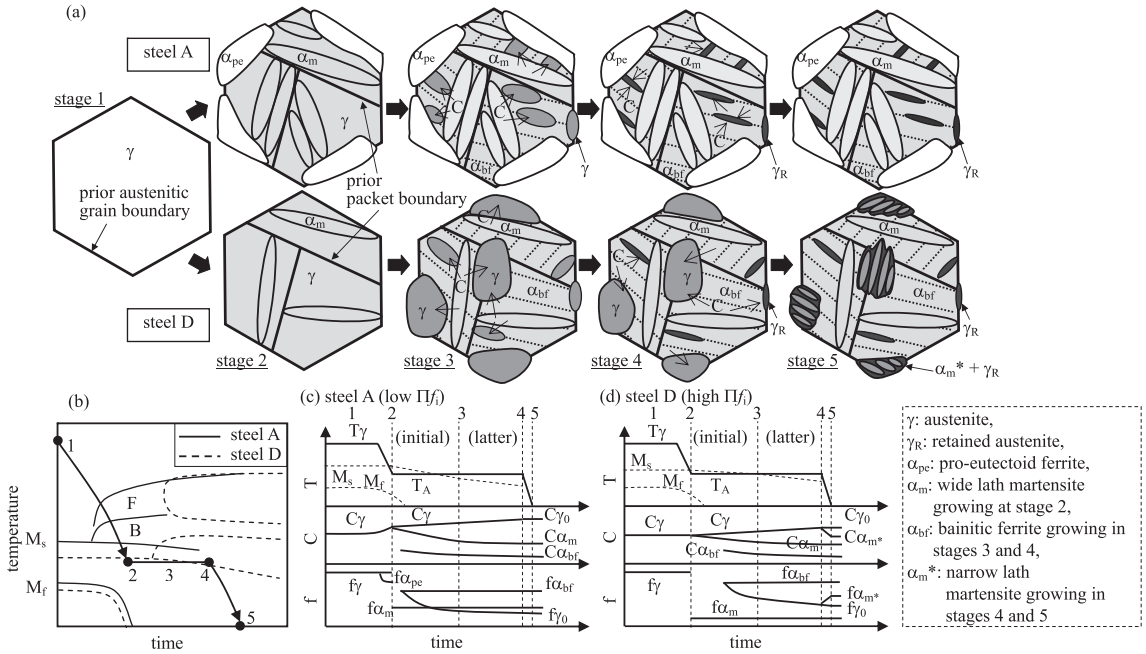

Fig. 13. Illustration of (a) microstructural change for steels A and D at stages 1 through 5, (b) heat treatment diagram, and (c) and (d) changes in martensite start temperature of austenite, carbon concentrations ($C\gamma$, $C\alpha_{bf}$, $C\alpha_m$ and $C\alpha_{m*}$) and volume fractions ($f\gamma$, $f\alpha_{pe}$, $f\alpha_{bf}$, $f\alpha_m$ and $f\alpha_{m*}$) of each phase during austempering at 350 or 400°C in steels A and D.

vol% in stage 2. Next, in stage 3, the untransformed austenite transforms to bainitic ferrite with carbon partitioning from martensite to austenite, although the volume fraction of the transformed bainitic ferrite is smaller than that in stage 3 for steel A, because of the delay in the bainite transformation due to the alloying elements. In this case, the carbon enrichment of austenite is incomplete (Fig. 10(b)). The incompletely carbon-enriched austenite changes to island-shaped martensite and retained austenite upon final quenching to room temperature. Then, the retained austenite is finer and is located along the narrow carbon-enriched lath martensite (α_m*) boundaries.

In Fig. 3, it was seen that the Vickers hardness of steels A–E increased with hardenability. This may be caused by the increase in volume fraction of the blocky second phase.

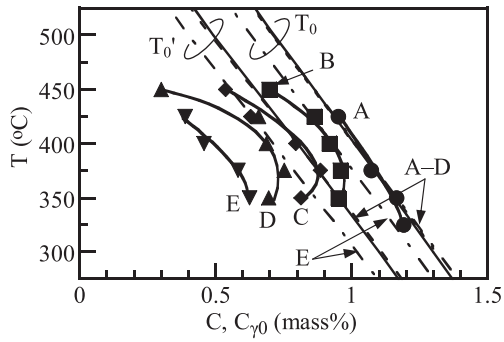

Fig. 14. Variations in T_0 and T_0' lines and measured carbon concentration of retained austenite in steels A–E. For calculation of the T_0' line, the strain energy was assumed to be 400 J/mole.

4.2. Effects of Chemical Composition on Retained Austenite Characteristics

In Figs. 10 and 11, the carbon concentration decreased with hardenability when the steels were austempered at 350 or 400°C for 1 000 s, although the volume fraction of the retained austenite increased with increasing hardenability. In general, the carbon concentration of the retained austenite is mainly controlled by the T_0 or T_0' temperatures, as well as by the morphology, size and carbon diffusion rate.[21)]

Figure 14 shows the T_0 and T_0' lines calculated by ThermoCalc, and the carbon concentrations of the retained austenite in steels A–E measured by X-ray diffractometry. The carbon concentration in steel A agrees quite well with the T_0 line. However, the carbon concentrations of steels B–E do not coincide with the T_0 line, although those of steels B–D agree with the T_0' line. In this case, Cr and/or Mo hardly influence the T_0 temperature, in contrast to Ni. Thus, the decreased carbon concentration of the retained austenite may be caused by the decreased carbon diffusion to austenite from the bcc phase or by incomplete carbon enrichment due to the delay in the ferrite or bainite transformation caused by additions of Cr, Mo and/or Ni. On the other hand, a considerable decrease in the carbon concentration upon Ni addition is considered to be associated principally with the lowered T_0 line, as well as the decreased carbon diffusion or incomplete carbon enrichment.

The highest carbon concentration of retained austenite in steel A may be caused by a sufficiently high diffusion rate of carbon from pro-eutectoid ferrite into austenite during cooling to the austempering temperature.

In Fig. 12, the k values increased slightly with hardenability factor in steels A–E austempered at 400°C, contrary to the hardenability dependence of the carbon concentration of the retained austenite (Figs. 10 and 11). According to Sugimoto *et al.*,[22)] the k values below about 5.0 in steels A–D indicate that they are stable enough, and can be regarded to have almost the same mechanical stability. As shown in Fig. 7, most of the retained austenite phases in the steels

with high hardenability factors are (i) very fine and (ii) located along narrow lath martensite boundaries in the blocky second phase, as well as on bainitic ferrite lath boundaries. Therefore, in spite of the lower carbon concentration of the retained austenite, the morphology constrained by narrow lath martensite may contribute to the relative stability of the retained austenite of steels B–D, with the exception of steel E.

5. Summary

The effects of alloying elements such as Cr, Mo and Ni on the microstructure and retained austenite characteristics of 0.2% C, 1.5% Si, 1.5% Mn and 0.05% Nb TBF steel were investigated. The results can be summarized as follows:

(1) When the TBF steels were austempered at temperatures in the ranges of M_S and M_f, the Vickers hardness increased from HV300 to HV430 with increasing hardenability. This was caused by an increase in the narrow lath martensite volume fraction.

(2) When Cr-, Mo- and/or Ni-bearing steels were austempered at temperatures lower than the M_S temperature, the volume fraction of the blocky second phase or M-A constituent (narrow lath martensite and retained austenite) increased, and the mixed matrix structure of lath bainitic ferrite and martensite was refined. Most of the retained austenite was considerably refined, and resided at narrow lath martensite interfaces in the blocky second phase and at formerly transformed bainitic ferrite and martensite lath boundaries.

(3) The volume fraction of the retained austenite in the TBF steels increased with increasing hardenability factor. In contrast, the carbon concentration decreased with increasing hardenability factor. This was associated with the decreased carbon diffusion to austenite from the bcc phase or incomplete carbon enrichment due to the retardation of the bainite transformation caused by additions of Cr, Mo and/or Ni. The addition of Ni further lowered the T_0 line. Although the carbon concentration of the retained austenite in the Cr- and/or Mo-bearing steels was low, the retained austenite stability against straining was sufficiently high for the TRIP effect to be observed.

Acknowledgements

This study was supported by the Grants from Adaptable and Seamless Technology Transfer Program through Target-driven R&D, the Japan Science and Technology Agency, and a Grant-in-Aid for Scientific Research (B) from the Ministry of Education, Science, Sports and Culture, Japan (No.2008-20360311).

REFERENCES

1) V. F. Zackay, E. R. Parker, D. Fahr and B. Bush: *Trans. Am. Soc. Met.*, **60** (1967), 252.
2) T. Furukawa: *Mater. Sci. Technol.*, **5** (1989), 465.
3) U. Brux, G. Frommeyer, O. Grassel, L. W. Meyer and A. Weise: *Steel Res.*, **73** (2002), 294.
4) W. Cao, J. Shi, C. Wang, L. Xu, M. Wang, Y. Weng and H. Dong: Proc. of ICAS 2010, Metall. Ind. Press, Beijing, (2010), 196.
5) J. G. Speer, D. V. Edomonds, F. C. Rizzo and D. K. Matlock: *Solid State Mater. Sci.*, **8** (2004), 219.
6) K. Sugimoto, J. Sakaguchi, T. Iida and T. Kashima: *ISIJ Int.*, **40** (2000), 920.
7) M. Murata, J. Kobayashi and K. Sugimoto: *Tetsu-to-Hagané*, **96** (2010), 84.
8) K. Sugimoto, M. Murata and S. Song: *ISIJ Int.*, **50** (2010), 162.
9) S. Song, K. Sugimoto, M. Kobayashi, H. Matsubara and T. Kashima: *Tetsu-to-Hagané*, **86** (2000), 563.
10) T. Hojo, K. Sugimoto, Y. Mukai and S. Ikeda: *ISIJ Int.*, **48** (2008), 824.
11) I. Tamura: Steel Material Study on the Strength, Nikkan Kogyo Shinbun Ltd., Tokyo, (1970), 40.
12) M. A. Grossman: *Trans. AIME*, **150** (1942), 227.
13) J. H. Hollomon and L. D. Jaffe: *Trans. AIME*, **167** (1946), 601.
14) H. Maruyama: *J. Jpn. Soc. Heat Treat.*, **17** (1977), 198.
15) D. J. Dyson and B. Holmes: *J. Iron Steel Inst.*, **208** (1970), 469.
16) D. P. Koistinen and R. E. Marburger: *Acta Metall.*, **7** (1959), 59.
17) O. Umezawa: *J. Jpn. Inst. Light Met.*, **50** (2000), 86.
18) B. N. P. Babu, M. S. Bhat, E. R. Parker and V. F. Zackay: *Metall. Trans. A*, **7A** (1976), 17.
19) D. Quidort and Y. J. M. Brechet: *Acta. Metall.*, **49** (2001), 4161.
20) M. Takahashi and H. K. D. Bhadeshia: *Mater. Trans. JIM*, **32** (1991), 689.
21) K. Sugimoto: *Mater. Sci. Technol.*, **25** (2009), 1108.
22) K. Sugimoto, N. Usui, M. Kobayashi and S. Hashimoto: *ISIJ Int.*, **32** (1992), 1311.